Available online at www.sciencedirect.com
SCIENCE DIRECT®
Nuclear Physics B (Proc. Suppl.) 141 (2005) 225–232
NUCLEAR PHYSICS B PROCEEDINGS SUPPLEMENTS
www.elsevierphysics.com

Spin-dependent parton distributions in the nucleon

I. C. Cloët[a], W. Bentz[b] and A. W. Thomas[c]

[a]Special Research Centre for the Subatomic Structure of Matter and
Department of Physics and Mathematical Physics, University of Adelaide, SA 5005, Australia

[b]Department of Physics, School of Science, Tokai University Hiratsuka-shi, Kanagawa 259-1292, Japan

[c]Jefferson Lab, 12000 Jefferson Avenue, Newport News, VA 23606, U.S.A.

Spin-dependent quark light-cone momentum distributions are calculated for a nucleon in the nuclear medium. We utilize a modified NJL model where the nucleon is described as a composite quark-diquark state. Scalar and vector mean fields are incorporated in the nuclear medium and these fields couple to the confined quarks in the nucleon. The effect of these fields on the spin-dependent distributions and consequently the axial charges is investigated. Our results for the "spin-dependent EMC effect" are also discussed.

1. INTRODUCTION

Quark distributions were among the first experimental confirmations of QCD and have played a fundamental role in our understanding of nucleon structure. However, a satisfactory theoretical understanding is still lacking. In particular, the non-perturbative aspects of these observables still remain largely unexplored, although lattice QCD has made some progress determining the first few moments [1–6].

Add to this modifications from the nuclear medium and you have a very challenging problem indeed, one that has caught the attention of both experimentalists and theorists since the European Muon Collaboration (EMC) reported their surprising results [7–9]. It was found that nuclear structure functions differ from those of the free nucleon by 10-20% in regions where Fermi motion was thought to be negligible. This has become known as the EMC effect [10].

In view of our inability to solve QCD directly, models are still indispensable for the investigation of the non-perturbative regime of the strong interaction and currently represent the only method with which to estimate nuclear medium modifications to QCD observables.

In this paper we determine the valence spin-dependent quark light-cone momentum distributions in a nuclear medium. The theoretical investigation of medium modifications to spin-dependent parton distributions (see *e.g.* [11–14]) has not experienced the same level of activity as their spin-independent counterparts. However, it is crucial to investigate these effects as they go to the very heart of our understanding of nuclear structure. From a purely practical point of view we need to know how to correctly extract neutron structure functions from nuclear data.

The formalism developed in Ref. [15] is used to incorporate the effects of the scalar and vector fields of the nuclear medium coupling to the quarks. The medium modifications to the free distributions are presented. The NJL model is utilized, where the nucleon is described as a quark-diquark bound state and the diquark is a qq bound state solution to the Bethe-Salpeter equation.

2. FINITE DENSITY QUARK DISTRIBUTIONS

The spin-dependent light-cone quark distribution per nucleon in a nucleus of mass number A is defined as

$$\Delta f_{q/A}\left(x_A\right) = \frac{P_-}{A^2}\int \frac{d\omega^-}{2\pi} e^{iP_-\, x_A\, \omega^-/A}$$

0920-5632/$ – see front matter © 2004 Published by Elsevier B.V.
doi:10.1016/j.nuclphysbps.2004.12.034

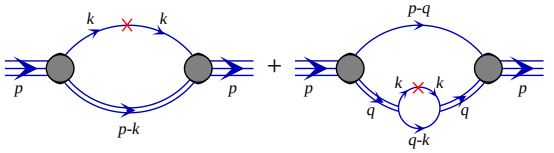

Figure 1. Feynman diagrams representing the spin-dependent quark distributions in the nucleon, needed to determine $\Delta f_{q/N}(x)$, given in Eq. (5). The single line represents the quark propagator and the double line the diquark t-matrix. The shaded oval denotes the quark-diquark vertex function and the operator insertion has the form $\gamma^+\gamma_5\,\delta\Big(x-\frac{k_-}{p_-}\Big)\,\frac{1}{2}\,(1\pm\tau_z)$. The second diagram, which we refer to as the "diquark diagram", symbolically stands for the two diagrams, each with the operator insertion on a different quark line within the diquark.

$$\langle A,P|\overline{\psi}(0)\,\gamma^+\gamma_5\,\psi(\omega^-)|A,P\rangle, \quad (1)$$

where ψ is the quark field and P^μ the 4-momentum of the nucleus. We work in the rest frame where $P^\mu = \big(M_A,\vec{0}\big)$. We assume that Eq. (1) can be expressed as the convolution integral

$$\Delta f_{q/A}\,(x_A) = \int dy_A \int dx\;\delta(x_A - y_A\,x)\;\Delta f_{q/N}(x)\;\Delta f_{N/A}(y_A)\,, \quad (2)$$

where $\Delta f_{q/N}(x)$ is the spin-dependent quark distribution in the nucleon and $\Delta f_{N/A}(y_A)$ the spin-dependent momentum distribution of the nucleon in the nucleus. There have been numerous investigations of $\Delta f_{N/A}$ [16] and it is straightforward to calculate for any particular nucleus. On the other hand, as our current interest concerns the new features of our model, namely the change in $\Delta f_{q/N}$ in-medium, we shall simply replace $\Delta f_{N/A}$ by the spin-independent quantity $f_{N/A}$, calculated in infinite nuclear matter. These distributions are defined by

$$\Delta f_{q/N}(x) = p_- \int \frac{d\omega^-}{2\pi} e^{ip_-\,x\,\omega^-} \langle N,p|\overline{\psi}(0)\,\gamma^+\gamma_5\,\psi(\omega^-)|N,p\rangle, \quad (3)$$

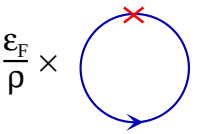

Figure 2. Feynman diagram representing the Fermi smearing function $f_{N/A}(y_A)$, given in Eq. (6). The solid line denotes the nucleon propagator, ε_F, ρ are the Fermi energy and baryon density, respectively, and the operator insertion has the form $\gamma^+\,\delta\Big(p_- - \frac{\varepsilon_F\,y_A}{\sqrt{2}}\Big)$.

$$f_{N/A}(y_A) = \frac{P_-}{A^2}\int \frac{d\omega^-}{2\pi} e^{iP_-\,y_A\,\omega^-/A} \langle A,P|\overline{\psi}_N(0)\,\gamma^+\psi_N(\omega^-)|A,P\rangle, \quad (4)$$

and can be expressed as [17–19]

$$\Delta f_{q/N}(x) = -i\int \frac{d^4k}{(2\pi)^4} \delta\Big(x-\frac{k_-}{p_-}\Big)\,\mathrm{Tr}\left(\gamma^+\gamma_5\,M(p,k)\right), \quad (5)$$

$$f_{N/A}(y_A) = -\frac{i}{A}\int \frac{d^4p}{(2\pi)^4} \delta\Big(y_A-\frac{A\,p_-}{M_A}\Big)\,\mathrm{Tr}\left(\gamma^+\,G_N(p)\right). \quad (6)$$

Here $M(p,k)$ is the quark two-point function in the nucleon and $G_N(p)$ the nucleon two-point function in the nucleus. Within any model that describes the nucleon as a bound state of quarks, these distribution functions can be associated with a straightforward Feynman diagram calculation, see Figs. 1 and 2, where the propagators include the scalar and vector fields.

An alternative to this direct calculation is provided in Ref. [15]. It is demonstrated that given a quark distribution in a free nucleon, the in-medium effect of the scalar field can be included via the effective masses. We will denote this quantity by $\Delta f_{q/N0}(x)$[1] The Fermi motion of the nucleon is then incorporated by convoluting $\Delta f_{q/N0}(x)$ with the "scalar-field" Fermi smearing

[1]The subscript 0 denotes the absence of any vector field, however such a distribution may include scalar fields and Fermi motion effects.

function, $f_{N/A0}(\tilde{y}_A)$, producing the distribution

$$\Delta f_{q/A0}(\tilde{x}_A) = \int d\tilde{y}_A \int dx \; \delta\left(\tilde{x}_A - \tilde{y}_A\, x\right) \Delta f_{q/N0}(x)\, f_{N/A0}(\tilde{y}_A). \quad (7)$$

Finally, the vector-field is included by simply scaling $\Delta f_{q/A0}(\tilde{x}_A)$, and shifting the Bjorken variable. The in medium structure function becomes

$$\Delta f_{q/A}\left(x_A\right) = \frac{\varepsilon_F}{E_F}\,\Delta f_{q/A0}\left(\tilde{x}_A = \frac{\varepsilon_F}{E_F}x_A - \frac{V_0}{E_F}\right), \quad (8)$$

where $\varepsilon_F = \sqrt{p_F^2 + M_N^2} + 3\,V_0 \equiv E_F + 3\,V_0$, p_F is the Fermi momentum and V_0 is the zeroth component of the vector field felt by a quark. In this discussion, the spin-dependent quark distribution in the nucleon, $\Delta f_{q/N0}(x)$, is determined from the Feynman diagrams of Fig. 1, where the propagators are the usual free ones but including the density dependent effective masses. The Fermi smearing function, $f_{N/A0}(\tilde{y}_A)$, is represented by the Feynman diagram in Fig. 2 with $\varepsilon_F \to E_F$, $y_A \to \tilde{y}_A$ and the nucleon propagator is given by

$$S_N(p) = i\pi\,\frac{\not{p} + M_N}{E_p}\,\delta(p_0 - E_p)\,\Theta(p_F - |\vec{p}|)\,. \quad (9)$$

We find [15]

$$f_{N/A0}(\tilde{y}_A) = \frac{3}{4}\left(\frac{E_F}{p_F}\right)^3\left[\left(\frac{p_F}{E_F}\right)^2 - (1-\tilde{y}_A)^2\right]. \quad (10)$$

The various distributions have support in the following regions

$$\Delta f_{q/N0}(x): \qquad 0 < x < 1, \quad (11)$$

$$f_{N/A0}\left(\tilde{y}_A\right): \qquad 1 - \frac{p_F}{E_F} < \tilde{y}_A < 1 + \frac{p_F}{E_F}, \quad (12)$$

$$\Delta f_{q/A0}\left(\tilde{x}_A\right): \qquad 0 < \tilde{x}_A < 1 + \frac{p_F}{E_F}, \quad (13)$$

$$\Delta f_{q/A}\left(x_A\right): \qquad \frac{V_0}{\varepsilon_F} < x_A < \frac{E_F + p_F + V_0}{\varepsilon_F}. \quad (14)$$

3. NUCLEAR MATTER AND THE NUCLEON IN THE NJL MODEL

The NJL model is a chiral effective quark theory that is characterized by a 4-Fermi contact interaction. Using Fierz transformations any 4-Fermi interaction can be expressed in the form $\sum_i G_i \left(\overline{\psi}\Gamma_i\psi\right)^2$, where the Γ_i are matrices in Dirac, colour and flavour space. The coupling constants G_i are functions of the original coupling appearing in the initial interaction Lagrangian.

We consider $\mathrm{SU}(2)_f$ NJL Lagrangians; writing explicitly those terms relevant to this discussion

$$\mathcal{L} = \overline{\psi}\left(i\,\partial\!\!\!/ - m\right)\psi \;+\; G_\pi\left(\left(\overline{\psi}\psi\right)^2 - \left(\overline{\psi}\gamma_5\,\vec{\tau}\psi\right)^2\right) \;-\; G_\omega\left(\overline{\psi}\gamma^\mu\psi\right)^2 + \ldots, \quad (15)$$

where we include the scalar, pseudoscalar and vector terms and m is the current quark mass. Separating the nuclear matter ground state expectation values of the quark bilinears as, $\overline{\psi}\Upsilon\psi = \langle\rho|\overline{\psi}\Upsilon\psi|\rho\rangle + :\overline{\psi}\Upsilon\psi:$, where $\Upsilon = \mathbb{1}, \gamma^\mu$, the Lagrangian can be expressed as

$$\mathcal{L} = \overline{\psi}\left(i\,\partial\!\!\!/ - M - \not{V}\right)\psi \;-\; \frac{(M-m)^2}{4\,G_\pi} + \frac{V_\mu V^\mu}{4G_\omega} + \mathcal{L}_I, \quad (16)$$

where we have defined $M = m - 2\,G_\pi\langle\rho|\overline{\psi}\psi|\rho\rangle$, $V^\mu = 2\,G_\omega\langle\rho|\overline{\psi}\gamma^\mu\psi|\rho\rangle$ and $\mathcal{L}_I$ is the normal ordered interaction Lagrangian.

In the NJL model the nucleon is constructed as a quark-diquark bound state and in this preliminary investigation we consider the scalar diquark $\left(J^\pi = 0^+, T = 0, \text{colour } \overline{3}\right)$ channel only. Using a further Fierz transformation the interaction Lagrangian can be expressed as a sum of qq interaction terms. The interaction in the scalar qq channel has the form

$$\mathcal{L}_{I,s} = G_s\left(\overline{\psi}\gamma_5\,C\,\tau_2\,\beta^A\,\overline{\psi}^T\right)\left(\psi^T\,C^{-1}\,\gamma_5\,\tau_2\,\beta^A\,\psi\right), \quad (17)$$

where $\beta^A = \sqrt{\frac{3}{2}}\,\lambda^A$ $(A = 2,5,7)$ are the colour $\overline{3}$ matrices and C is the charge conjugation matrix, $C = i\gamma_2\gamma_0$.

The reduced t-matrix in the scalar qq channel is obtained by solving the appropriate Bethe-Salpter equation, giving

$$\tau_s(q) = \frac{4iG_s}{1 + 2\,G_s\,\Pi_s(q^2)}. \tag{18}$$

The scalar qq bubble graph has the form

$$\Pi_s(q^2) = 6i \int \frac{d^4k}{(2\pi)^4}\,\mathrm{Tr}\Big[\gamma_5\,S(k)\,\gamma_5\,S(k-q)\Big], \tag{19}$$

and $S(q) = 1/\not{q} - M + i\varepsilon$ is the Feynman propagator for the constituent quark mass and the trace is over Dirac indices.

Restricted to the scalar qq interaction the Faddeev equation for the nucleon can be reduced to an effective Bethe-Salpeter equation for a composite scalar diquark and quark interacting via quark exchange. At finite density the gap equation develops a dependence on the nucleon mass, which greatly complicates solving the Bethe-Salpeter equation. Therefore, for this initial investigation, we restrict ourselves to the static approximation to the Faddeev equation, where the propagator in the quark exchange kernel is replaced by $-1/M$. This permits a ready solution to the effective Bethe-Salpeter equation, with the nucleon t-matrix in the colour singlet channel having the form

$$T(p) = \frac{3}{M}\frac{1}{1 + \frac{3}{M}\,\Pi_N(p)}, \tag{20}$$

where the quark-diquark bubble graph is given by

$$\Pi_N(p) = -\int \frac{d^4k}{(2\pi)^4}\,S(k)\,\tau_s(p-k). \tag{21}$$

The nucleon and scalar diquark masses are obtained as separate solutions to the equations

$$1 + \frac{3}{M}\,\Pi_N(\not{p} = M_N) = 0, \tag{22}$$

$$1 + 2\,G_s\,\Pi_s(q^2 = M_s^2) = 0, \tag{23}$$

which manifest as poles in the corresponding t-matrices.

The nucleon vertex function, $\Gamma_N(p)$, in the noncovariant light-cone normalization is defined by the pole behaviour of Eq. (20)

$$T(p) \overset{p_+ \to \tilde{\varepsilon}_p}{\longrightarrow} \frac{\Gamma_N(p)\,\overline{\Gamma}_N(p)}{p_+ - \tilde{\varepsilon}_p}, \tag{24}$$

where $\tilde{\varepsilon}_p$ is the light-cone energy. We find[2]

$$\Gamma_N(p) = \sqrt{-Z_N\frac{M_N}{p_-}}\,u_N(p), \tag{25}$$

$$Z_N = \frac{-1}{\partial\Pi_N(p)/\partial\not{p}}\bigg|_{\not{p}=M_N}. \tag{26}$$

The free nucleon Dirac spinor is normalized as $\overline{u}_N u_N = 1$.

The effective potential for nuclear matter can be rigorously derived for any NJL Lagrangian using hadronization techniques. This results in a complicated nonlocal effective Lagrangian, that in principle can be applied to nuclear matter. Using the mean-field approximation and ignoring diquark and baryon "trace log terms" in the effective Lagrangian we obtain the following effective potential from Eq. (16)

$$\mathcal{E} = \mathcal{E}_V - \frac{V_0^2}{4G_\omega} + \int \frac{d^3p}{(2\pi)^2}\,\Theta\left(p_F - |\vec{p}|\right)\varepsilon_p, \tag{27}$$

where $\varepsilon_p = \sqrt{\vec{p}^2 + M_N^2} + 3\,V_0$ and the vacuum contribution is

$$\mathcal{E}_V = 12i \int \frac{d^4k}{(2\pi)^4}\ln\left(\frac{k^2 - M^2 + i\varepsilon}{k^2 - M_0^2 + i\varepsilon}\right) + \frac{(M-m)^2}{4G_\pi} - \frac{(M_0-m)^2}{4G_\pi}, \tag{28}$$

where we consider nuclear matter at rest. The zeroth component of the vector field can be replaced by the density as

$$\frac{\partial\mathcal{E}}{\partial V_0} = 0 \quad\Longrightarrow\quad V_0 = 6\,G_\omega\,\rho, \tag{29}$$

and the constituent quark mass M, for a fixed density, follows from the condition $\frac{\partial\mathcal{E}}{\partial M} = 0$.

[2] We adopt the Kogut-Soper convention for the light-cone variables where $a^\pm = \frac{1}{\sqrt{2}}\left(a^0 \pm a^3\right)$ and $a_\pm = \frac{1}{\sqrt{2}}\left(a_0 \pm a_3\right)$, therefore $a^\pm = a_\mp$.

4. REGULARIZATION AND THE EVALUATION OF THE QUARK DISTRIBUTIONS

As with any non-renormalizable theory a regularization prescription must be specified to fully define the model. We choose the proper-time regularization scheme [20–22], where loop integrals of products of propagators are evaluated by introducing Feynman parameters, Wick rotating and making the denominator replacement

$$\frac{1}{X^n} = \frac{1}{(n-1)!}\int_0^\infty d\tau\,\tau^{n-1}\,e^{-\tau X} \longrightarrow \frac{1}{(n-1)!}\int_{1/(\Lambda_{UV})^2}^{1/(\Lambda_{IR})^2} d\tau\,\tau^{n-1}\,e^{-\tau X}. \quad (30)$$

Ultraviolet (UV) and infrared (IR) cutoffs are introduced, the IR cutoff plays the role of eliminating unphysical thresholds for hadrons decaying into quarks, hence simulating confinement [21].

As the minus component of the quark momentum is fixed in Eq.(6), a direct evaluation of the quark distributions is not possible from the Feynman diagrams in a Euclidean formulation. Hence we consider first the moments

$$A_n = \int_0^1 dx\,x^{n-1}\,f_{q/N0}(x), \quad (31)$$

and from these reconstruct the distributions exactly. Further discussion of this method can be found in Ref. [23].

The quark diagram of Fig. 1 gives the following contribution to $\Delta f_{q/N0}$:

$$\Delta f^{(Q)}_{q/N0} = \overline{\Gamma}_N \int \frac{d^4k}{(2\pi)^4} \delta\!\left(x - \frac{k_-}{p_-}\right) S(k)\gamma^+\gamma_5 S(k)\,\tau_s(p-k)\,\Gamma_N. \quad (32)$$

Using Eq. (31)

$$A^{(Q)}_n = \overline{\Gamma}_N \int \frac{d^4k}{(2\pi)^4} \left(\frac{k_-}{p_-}\right)^{n-1} S(k)\gamma^+\gamma_5 S(k)\,\tau_s(p-k)\,\Gamma_N. \quad (33)$$

Evaluating the matrix elements and introducing a Feynman parameter we obtain[3]

$$A^{(Q)}_n = 2i\,g_s\,Z_N \int_0^1 d\alpha\,\alpha^{n-1}\,(1-\alpha) \int \frac{d^4k}{(2\pi)^4}\,\frac{(\alpha\,M_N + M)^2 - \vec{k}^2_\perp}{\left(k^2 - A + i\varepsilon\right)^3}, \quad (34)$$

where $A = \alpha(\alpha-1)p^2 + \alpha\,M_s^2 + (1-\alpha)M^2$. From the definition of the moments, Eq. (31), and introducing the proper-time regularization it is easy to show

$$\Delta f^{(Q)}_{q/N0}(x) = \frac{g_s\,Z_N}{16\pi^2}\,(1-x) \int_{1/(\Lambda_{UV})^2}^{1/(\Lambda_{IR})^2} d\tau\,\left[(xM_N + M)^2 - \frac{1}{\tau}\right] e^{-\tau A}. \quad (35)$$

The diquark diagram, $\Delta f^{(D)}_{q/N0}$, is evaluated in an analogous manner, however a trace of an odd number of γ-matrices with a γ_5 appears because of the operator insertion in the qq loop in the diquark propagator. Hence, with scalar diquark correlations only, we have

$$\Delta f^{(D)}_{q/N0} = 0. \quad (36)$$

In terms of $\Delta f^{(Q)}_{q/N0}$ and $\Delta f^{(D)}_{q/N0}$, the zero density, longitudinally polarized, spin-dependent valence quark distributions are given by

$$\Delta u_V(x) = \Delta f^{(Q)}_{q/N0} + \frac{1}{2}\Delta f^{(D)}_{q/N0}, \quad (37)$$

$$\Delta d_V(x) = \frac{1}{2}\Delta f^{(D)}_{q/N0}, \quad (38)$$

where all quantities involve the free (zero density) masses. Because we include only the scalar diquark channel at this stage we see from Eq. (36) that $\Delta d_V(x) = 0$.

5. RESULTS

The free parameters of the model are Λ_{IR}, Λ_{UV}, M_0, G_π, G_s and G_ω. These are determined as follows; the infrared cutoff is fixed at

[3] In this calculation we have used the a pole approximation for the diquark t-matrix, $\tau_s \to 4\,i\,G_s - \frac{i\,g_s}{q^2 - M_s^2 + i\,\varepsilon}$, where g_s is the residue at the mass pole of the full τ_s and is given by $g_s = \frac{-2}{\partial\,\Pi_s(q^2)/\partial q^2}\Big|_{q^2=M_s^2}$.

Table 1
List of the effective masses of the constituent quark M, diquark M_s, and nucleon M_N, at three different densities. The strength of the vector field V_0, the Fermi energy ε_F, and the mass per nucleon $\overline{M}_N = M_{N0} - \frac{E_B}{A}$ are also given.

	$\rho = 0\,\mathrm{fm}^{-3}$	$\rho = 0.16\,\mathrm{fm}^{-3}$	$\rho = 0.22\,\mathrm{fm}^{-3}$
M	400	308	276
M_s	576	413	355
M_N	940	707	634
V_0	0	53	75
ε_F	940	914	923
$\overline{M}_N$	940	925	923

$\Lambda_{IR} = 200$ MeV; the constituent quark mass at zero density is fixed at $M_0 = 400$ MeV; the ultraviolet cutoff Λ_{UV} is then obtained by requiring $f_\pi = 93$ MeV and $m_\pi = 140$ MeV; G_π then follows from m_π; and the coupling G_s is determined by requiring the nucleon mass at zero density to equal its physical value, $M_{N0} = 940$ MeV. Finally the coupling G_ω is determined such that the curve describing the nuclear matter binding energy per nucleon as a function of the density, pass through the empirical point of $(\rho,\ E_B/A) = \big(0.16\ \mathrm{fm}^{-3},\ 15\ \mathrm{MeV}\big)$. We find $\Lambda_{UV} = 638.5$ MeV, $G_\pi = 19.60\ \mathrm{GeV}^{-2}$, $G_s = 9.96\ \mathrm{GeV}^{-2}$ and $G_\omega = 7.25\ \mathrm{GeV}^{-2}$.

With G_ω the only free parameter for nuclear matter this model is unable to reproduce the empirical saturation point, instead saturation occurs at $(\rho,\ E_B/A) = \big(0.22\ \mathrm{fm}^{-3},\ 17.3\ \mathrm{MeV}\big)$. Consequently, as Eq. (8) is only valid at saturation [15], we must use the model saturation density for our numerical calculations. However, we include some results in Table 1 for $\rho = 0.16\,\mathrm{fm}^{-3}$ for comparison.

Table 1 lists the values of the effective masses, the strength of the vector field, the nucleon Fermi energy and the mass per nucleon $\overline{M}_N = M_{N0} - \frac{E_B}{A}$ for the three values of the density.

Our results for the free ($\rho = 0$) longitudinally polarized valence u-quark distribution, $\Delta u_V(x)$, are presented in Fig. 3. The solid line is the model prediction, at a scale of $Q^2 = 0.16\ \mathrm{GeV}^2$.

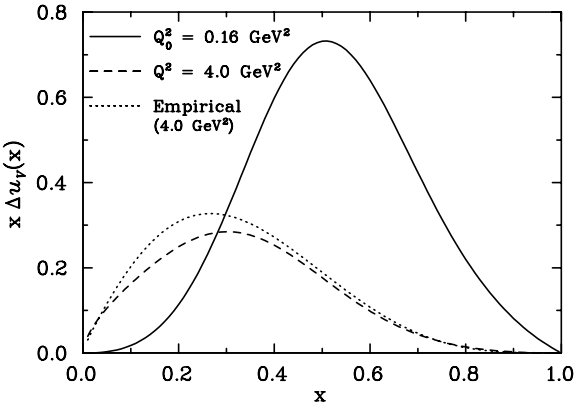

Figure 3. Zero density spin-dependent valence u-quark distribution multiplied by Bjorken x. The solid line is the model prediction at the NJL scale of $Q_0^2 = 0.16\ \mathrm{GeV}^2$ and the dashed line is the result after QCD evolution to a scale of $Q^2 = 4.0\ \mathrm{GeV}^2$. The dotted line is the empirical parametrization of Ref. [25], at a scale of $Q^2 = 4.0\ \mathrm{GeV}^2$.

We have chosen to use the same Q^2 scale as Ref. [15], where it was found that the empirical spin-independent quark distributions are, after Q^2 evolution[4], best reproduced with a model scale of $Q^2 = Q_0^2 = 0.16\ \mathrm{GeV}^2$. The QCD evolution is performed according to the Dokshitzer-Gribov-Lipatov-Alterelli-Parisi (DGLAP) equations, and we compare our results to the empirical parametrization of Ref. [25] at a scale of $4\ \mathrm{GeV}^2$. The model and empirical parameterizations are given in Fig. 3 as the dashed and dotted lines respectively. It is clear that the model results reproduce the qualitative features of the empirical result, with the peak shifted slightly to larger x.

In this scalar diquark NJL model the longitudinally polarized valence d-quark distribution, $\Delta d_V(x)$, is zero everywhere (see Eqs. (38,36)). The Bjorken sum rule derived from current algebra implies that the isovector spin combination Δq_3 equals g_A the isovector axial charge of the nucleon, with an experimental value of

[4] We utilize the computer code of Ref. [24] to perform the Q^2 evolution. We choose $N_f = 3$, $\Lambda_{\mathrm{QCD}} = 250$ MeV in the $\overline{\mathrm{MS}}$ renormalization scheme up to NLO in the perturbative expansion.

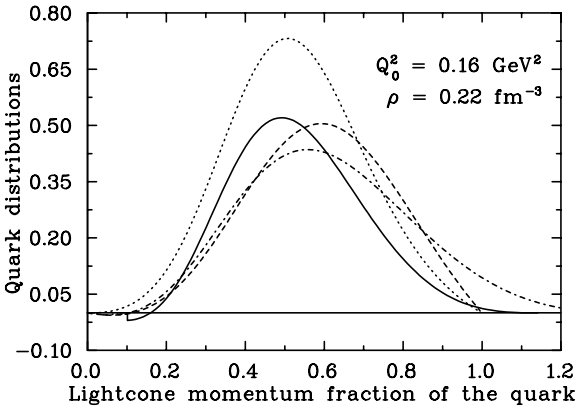

Figure 4. All results presented here are at the model scale, $Q_0^2 = 0.16$ GeV^2 and each distribution is plotted with respect to the appropriate Bjorken scaling variable. The dotted line is $x\,\Delta u_V(x)$ in the free nucleon, the dashed line illustrates the effect of replacing the free masses with the effective ones. This distribution convoluted with the Fermi smearing function of Eq. 7, is presented as the dot-dash line and the final result where the vector field is also included via the scale transformation Eq. 8, is represented by the solid line.

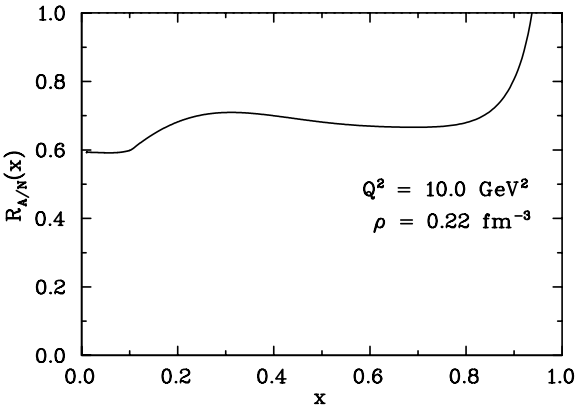

Figure 5. Ratio of $\Delta u_V(x_A)$ in the nuclear medium to $\Delta u_V(x)$ in the free nucleon, at the model saturation density and $Q^2 = Q_0^2$. We are able to plot this ratio as a function of x with the use of the relation $x_A = \frac{M_{N0}}{\varepsilon_F} x = 1.02x$. Recall, M_{N0} is the nucleon mass at zero baryon density, hence $M_{N0} = 940$ MeV.

$g_A = 1.257 \pm 0.004$. Comparing to our result $\Delta q_3 = \Delta u_V = 0.685$, we see that the model prediction for g_A is a factor of 2 too small. The reason this simple model is unable to reproduce the experimental g_A is primarily the absence of the d-quark distribution. We also note that the empirical zeroth moment of the u_V distribution is $\Delta u_V = 0.940 \pm 0.26$ [25].

The results for the finite density spin-dependent quark distribution are presented in Fig. 4. The effect of the scalar field on the free distributions is obtained by simply replacing the free quark, diquark and nucleon mass, in Eq. (37), with their effective ones given in Table 1, the result is the dashed line. Evaluating the convolution integral, Eq. (7), including the Fermi smearing function given in Eq. (10), incorporates the Fermi motion of the nucleon. The resulting distribution is the dot-dashed line in Fig. 4. The effect of the vector field is now trivially determined from the scale transform of Eq. (8), and is indicated by the solid line in Fig. 4. The dotted line is simply the zero density result given in Fig. 3 and is included here for comparison.

The introduction of the scalar field significantly reduces Δu_V, resulting in a reduced strength for the axial couplings – we find $g_A = 0.435$. With the inclusion of Fermi motion there is a depletion at intermediate x and the support now extends beyond $x = 1$. This is possible because of momentum sharing between the nucleons up to the Fermi surface. The axial vector charge now becomes slightly larger, having the value $g_A = 0.441$.

Finally, the effect of the vector field is to squeeze the distribution from large x, pushing the peak to smaller x and reducing the region of support. As the introduction of the vector field is achieved via a simple scale transformation, which is associated with a gauge transformation in Ref. [15], the value of the zeroth moment and hence g_A remains unchanged from the previous case.

The curve in Fig. 5 is the ratio of the nuclear and nucleon spin-dependent u-quark distributions

$$R_{A/N}(x) = \frac{\Delta u_V(x_A)}{\Delta u_V(x)} \tag{39}$$

where the relation $x_A = \frac{M_{N0}}{\varepsilon_F} x = 1.02x$ is used to obtain $R_{A/N}(x)$ as a function of x only. The ratio exhibits a plateau between about $x = 0.4$ to $x = 0.8$ with an average value of about 0.7, and if we compare this to the corresponding result for the spin-independent case, we expect that the medium modifications are more significant for the spin-dependent structure functions. For more quantitative conclusions, however, we have to include in addition also the axial vector diquark channel.

6. CONCLUSION

Nuclear medium modifications to the spin-dependent quark light-cone momentum distributions have been discussed. We find that the medium effects are significant, more so than the spin-independent case, discussed in Ref. [15], where the same formalism was used. However, in this scalar diquark NJL model the longitudinally polarized valence d-quark distribution, $\Delta d_V(x)$, is zero everywhere. Hence, meaningful comparisons with experimental values for the Bjorken and Ellis-Jaffe sum rules, for example, are not possible in this simple model. It is clear that axial-vector diquark correlations must be included if a more complete description of spin-dependent distributions is to be realized in the NJL framework. These results will be forthcoming shortly.

This work was supported by the Australian Research Council and DOE contract DE-AC05-84ER40150, under which SURA operates Jefferson Lab, and by the Grant in Aid for Scientific Research of the Japanese Ministry of Education, Culture, Sports, Science and Technology, Project No. C2-16540267.

REFERENCES

1. G. Martinelli and C. T. Sachrajda, Phys. Lett. B **217**, 319 (1989).
2. D. Dolgov *et al.* [LHPC collaboration], Phys. Rev. D **66**, 034506 (2002).
3. M. Gockeler *et al.*,, Phys. Rev. D **53**, 2317 (1996).
4. M. Fukugita, Y. Kuramashi, M. Okawa and A. Ukawa, Phys. Rev. Lett. **75**, 2092 (1995).
5. S. Sasaki, K. Orginos, S. Ohta and T. Blum [the RIKEN-BNL-Columbia-KEK Collaboration], Phys. Rev. D **68**, 054509 (2003).
6. W. Detmold, W. Melnitchouk, J. W. Negele, D. B. Renner and A. W. Thomas, Phys. Rev. Lett. **87**, 172001 (2001).
7. J. J. Aubert *et al.* [European Muon Collaboration], Phys. Lett. B **123**, 275 (1983).
8. A. Bodek *et al.*, Phys. Rev. Lett. **51**, 534 (1983).
9. R. G. Arnold *et al.*, Phys. Rev. Lett. **52**, 727 (1984).
10. D. F. Geesaman, K. Saito and A. W. Thomas, Ann. Rev. Nucl. Part. Sci. **45**, 337 (1995).
11. A. W. Thomas, arXiv:hep-ph/9410335.
12. F. C. Khanna and A. Y. Umnikov, arXiv:hep-ph/9609356.
13. F. M. Steffens, K. Tsushima, A. W. Thomas and K. Saito, Phys. Lett. B **447**, 233 (1999).
14. A. Sobczyk and J. Szwed, Acta Phys. Polon. B **32**, 2947 (2001).
15. H. Mineo, W. Bentz, N. Ishii, A. W. Thomas and K. Yazaki, Nucl. Phys. A **735**, 482 (2004).
16. K. Saito, M. Ueda, K. Tsushima and A. W. Thomas, Nucl. Phys. A **705**, 119 (2002).
17. R. L. Jaffe, MIT-CTP-1261 *Lectures presented at the Los Alamos School on Quark Nuclear Physics, Los Alamos, N.Mex., Jun 10-14, 1985.*
18. V. Barone, A. Drago and P. G. Ratcliffe, Phys. Rept. **359**, 1 (2002).
19. J. R. Smith and G. A. Miller, Phys. Rev. C **65**, 055206 (2002).
20. D. Ebert, T. Feldmann and H. Reinhardt, Phys. Lett. B **388**, 154 (1996).
21. G. Hellstern, R. Alkofer and H. Reinhardt, Nucl. Phys. A **625**, 697 (1997).
22. W. Bentz and A. W. Thomas, Nucl. Phys. A **696**, 138 (2001).
23. N. Ishii, arXiv:nucl-th/0306028.
24. M. Hirai, S. Kumano and M. Miyama, Comput. Phys. Commun. **108**, 38 (1998).
25. M. Hirai, S. Kumano and N. Saito Phys. Rev. D **69**, 054021 (2004).